Earthquake Engineering, Tenth World Conference © 1992 Balkema, Rotterdam. ISBN 90 5410 060 5

Nonlinear numerical simulation of two-dimensional soil structure model test by shaking table

K. Nishi & M. Kanatani
Central Research Institute of Electric Power Industry, Japan

ABSTRACT : This paper describes the results of numerical simulation of shaking table tests on a two-dimensional soil-structure interaction system to verify a newly-developed nonlinear-response analytical method. The code is based on Biot's theory concerning saturated porous media, and a constitutive relation deduced from elasto-plastic theory to simulated the nonlinear deformation behavior of soils. The input material constants were decided carefully by specially arranged soil tests under very low confining pressures. The results of the numerical simulation were in good agreement with those of shaking table tests, especially for the acceleration, pore water pressure and settlement time histories.

1. INTRODUCTION

So far numerous analytical procedures have been developed by many researchers. In particular, complex response analyses in the frequency domain based on the equivalent linear concept have been used frequently in actual aseismic design. However, dynamic analytical codes that calculate the nonlinear behavior of soils in the time domain have been developed recently to predict precisely the deformation behaviour of ground with failure phenomena such as liquefaction in sandy layers under strong earthquake motion.

We have also developed a nonlinear response analytical code based on the effective stress concept to predict the deformation of foundation ground in two-dimensional fields. The elasto-plastic constitutive relation is introduced in this code to simulate the nonlinearity of soils under multi-dimensional cyclic stress conditions. We compare shaking table test results for a model structure embedded in sandy ground and the numerical simulation results to verify our method.

2. CONSTITUTIVE RELATIONS

The features of the constitutive relations used are as follows (Nishi and Kanatani 1990):

1) Masing rule is used to evaluate the hysteretic curves during cyclic shear loading under multi-dimensional stress conditions for the relationship between the effective stress ratio and deviatoric strain.

2) The non-associated flow rule is applied to predict the stress versus plastic strain relations.

3) The stress parameter η^* defined by Sekiguchi and Ohta (1977) is introduced to express the plastic deformation behavior during cyclic loading under general stress conditions.

4) The yield function f is defined as:

$$\text{if } \eta^* \geq \eta^*_{max} \quad f = \eta^* \tag{1}$$

$$\text{if } \eta^* < \eta^*_{max} \quad ; f = \eta^*_r \tag{2}$$

where η^*_{max} is the maximum value of η^* previously experienced and η^*_r means η^* after the reverse in cyclic shear loading.

5) The plastic potential function g is deduced from the following stress-dilatancy equations.

$$\text{if } \eta^* \geq \eta^*_{max} \; ; \quad \frac{dV_d}{\sqrt{2I_2}} = M_m - \eta^* \tag{3}$$

$$\text{if } \eta^* < \eta^*_{max} \; ; \quad \frac{dV_d}{\sqrt{2I_2}} = \alpha\,(M_m - \eta^*_r) \tag{4}$$

where dV_d, $\sqrt{2I_2}$, M_m, and α are the plastic volumetric strain increment due to dilatancy, the second invariant of plastic deviatoric strain increment, the value of η^* at $dV_d = 0$, and the parameter dependent on the loading history, respectively.

There are seven fundamental material constants involved in this constitutive relationship and these can be determined easily by ordinal laboratory soil tests.

3. DYNAMIC ANALYTICAL METHOD

The newly-developed code is called NAFSS (Nonlinear Analysis of Fluid Solid System) and its main features are as follows:

3.1 Fundamental Equations of Two-Phase System

The fundamental equations for a two-phase system such as soil are as follows:

$$\sigma_{ij,j} + \rho g_i = \rho \ddot{u}_i + \rho_f \ddot{w}_i \tag{5}$$

$$-P_{,i} + \rho_f g_i = k_{ij}^{-1} \rho_f \dot{w}_j + \rho_f \ddot{u}_i + n^{-1} \rho_f \ddot{w}_i \tag{6}$$

$$w_{i,i} = \varepsilon_{ii} - (1-n) P k_s^{-1} - n P k_f^{-1} - \sigma_{ii}' (3k_s)^{-1} \tag{7}$$

$$\varepsilon_{ij} = (u_{i,j} + u_{j,i})/2 \tag{8}$$

$$\sigma_{ij} = \sigma_{ij}' - \alpha \delta_{ij} P = D_{ijkl} \varepsilon_{kl} - \alpha \delta_{kl} P \tag{9}$$

where σ : total stress
P : pore pressure
σ' : effective stress
u : displacement of solid skeleton
w : relative displacement of fluid to solid skeleton
ρ, ρ_f : density of soil and fluid
k : permeability
ε : strain of soil
g_i : body force
δ_{ij}: Kronecker's delta
n : porosity
k_s, k_f : bulk modulus of solid and fluid

The above equations were discretized by the Galerkin method to give the following matrix equation (Ghaboussi 1971).

$$\begin{bmatrix} M_s & M_c \\ M_c^T & M_f \end{bmatrix} \begin{bmatrix} \ddot{u} \\ \ddot{w} \end{bmatrix} + \begin{bmatrix} C^R & 0 \\ 0 & H \end{bmatrix} \begin{bmatrix} \dot{u} \\ \dot{w} \end{bmatrix} + \begin{bmatrix} K & C \\ C^T & E \end{bmatrix} \begin{bmatrix} u \\ w \end{bmatrix} = \begin{bmatrix} F \\ G \end{bmatrix} \tag{10}$$

Matrices F and G are the body force and surface traction acting on the mixed material and fluid, respectively.

3.2 Time Integration Method

We adopted the implicit-explicit hybrid time integration method (Hughes et al 1978) to solve the equation of motion with high accuracy. Eq. (12), which is the transformed equation of motion (11), is solved by this method.

$$M \cdot a^{n+1} + C \cdot v^{n+1} + K \cdot d^{n+1} = F^{n+1} \tag{11}$$

$$M \cdot a^{n+1} + C_i \cdot v^{n+1} + C_e \cdot v^{n+1} + K_i \cdot d^{n+1} + K_e \cdot d^{n+1} = F^{n+1} \tag{12}$$

where $C = C_i + C_e$, $K = K_i + K_e$

$$d^{n+1} = d^n + \Delta t \cdot v^n + \frac{\Delta t^2}{2} \cdot (1 - 2\beta) \cdot a^n \tag{13}$$

$$v^{n+1} = v^n + \Delta t (1 - 2\gamma) \cdot a^n \tag{14}$$

$$d^{n+1} = d^{n+1} + \Delta t^2 \cdot \beta \cdot a^{n+1} \tag{15}$$

$$v^{n+1} = v^{n+1} + \Delta t \cdot \gamma \cdot a^{n+1} \tag{16}$$

subscript i and e mean the implicit group and the explicit group, respectively.

4. NUMERICAL SIMULATION

4.1 Shaking Table Test

A 120-ton large shaking table owned by CRIEPI was used. A soil container with a width, height and depth of 6 m, 1 m and 1 m, respectively, was fixed on the table. Gifu sands with a water of 10% were put in the container and model ground with a relative density of about 70% was made-up by the tamping method. A structural model with a width, height and depth of 0.6 m, 0.6 m and 0.8 m, respectively, was buried in the ground to 0.4 m from ground surface. Accelerometers, pore pressure gauges and displacement transducers were set in the ground or on the structure model as shown in Fig. 1. Water was supplied from the bottom of the container but we think the saturation of ground was fairly low. The soil container was then shaken horizontally by an electro-hydraulic servo system. The input motion is shown in Fig. 2.

4.2 Analytical Model

The analytical model for the numerical simulation is shown in Fig. 1 as a finite mesh; the locations of the measuring instruments are also shown, where A, W and D mean the accelerometer, pressure gauge and displacement gauge, respectively. The horizontal ground width in the experiment is 6 m but it is reduced by 3 m in the analysis to shorten the calculation time.
The ground-deformation boundary conditions are fixed for the bottom, and viscous for both

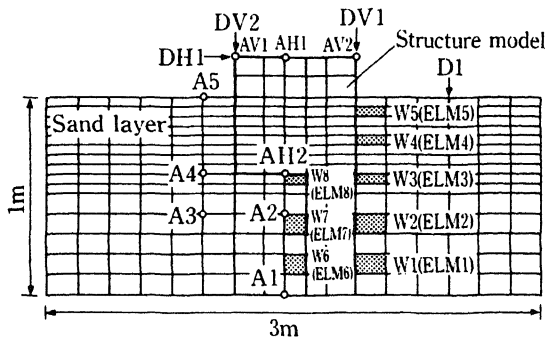

Fig.1 Schematic figure of shaking table test.

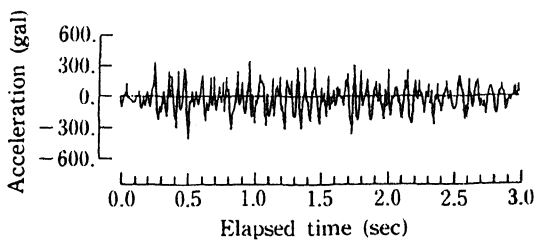

Fig.2 Input acceleration time history.

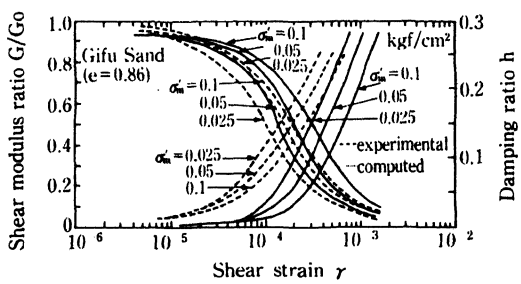

Fig.3 Comparison between computed and experimental results on G/Go ~ γ and h~ γ curves.

sides. The side and bottom surfaces of the buried part of the structure are completely connected with the soil. The permeability boundary conditions are permeable only for the ground surface; the other surfaces are impermeable.

4.3 Input Material Constants

Undrained cyclic triaxial tests were performed to determine the input material constants of the sand used in shaking-table tests.
The tests were performed under a very low confining pressure range of 0.025 kgf/cm² to 0.1 kgf/cm².

The comparisons between experiments and

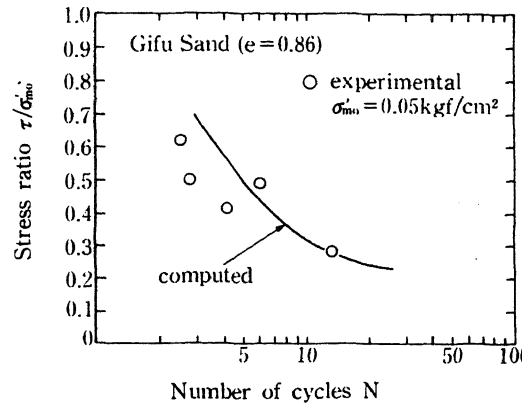

Fig.4 Comparison between computed and experimental results on the dynamic strength.

calculation by using constitutive relations for the dynamic deformation and strength characteristics are shown in Figs. 3 and 4, respectively. The dry mass density of the soil is 1.463 gf/cm³, and the internal friction angle at failure, and the mobilized friction angle at maximum contraction are 39° and 30° , respectively, for all layers. K_s is 3.7 X 10^4 kgf/cm² and K_r is 0.5 kgf/cm².
The permeability coefficient of soil k is assumed to be 10^{-2} cm/s. Young's modulus and Poisson's ratio of the structural model are 20000 kgf/cm² and 0.4, respectively. It is shown that the computed results concerning the shear strain dependency on shear modulus and liquefaction strength were in good agreement with the experimental results.

4.4 Time Integration

Time integration was conducted by the implicit-explicit hybrid method. The part of model ground is solved as the explicit one and only the structural model is solved as the implicit. The integration constants β , γ are 0.25 and 0.5, respectively. The integration time interval is 10^{-4} s.

4.5 Results

The experimental and computed acceleration time histories are compared in Fig. 5. Also, the experimental and computed results on the maximum acceleration values are shown in Fig. 6.

The calculated maximum accelerations are smaller than the experimental ones because the calculated wave was filtered by a 50 Hz to cut the high-frequency components that often occur in nonlinear dynamic analysis. However, the phases of the waves are in good agreement.

Figure 7 shows the time histories of the structure settlement. The calculated settlements are fairly large compared to the

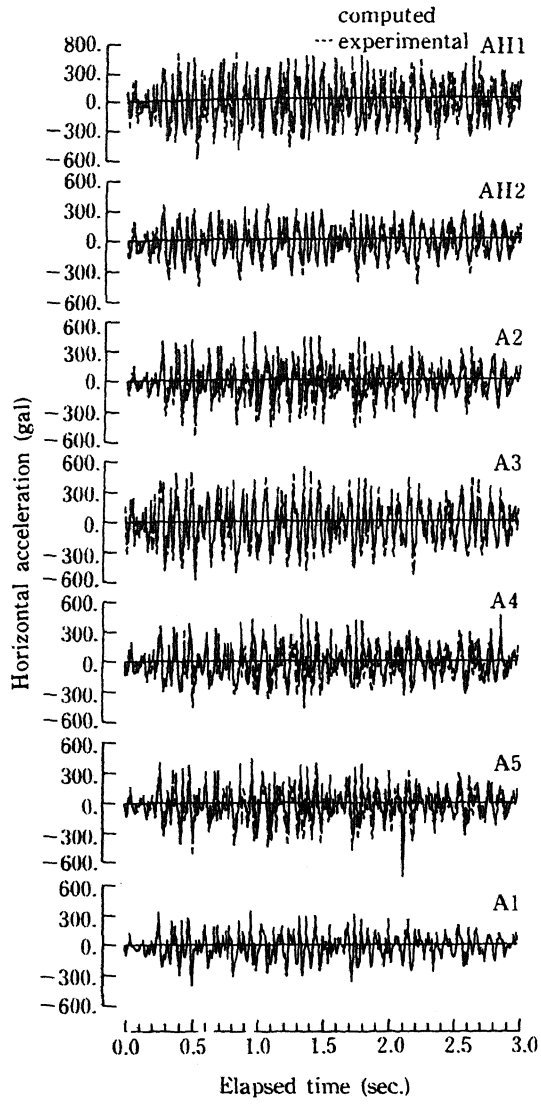

Fig.5 Comparison between computed and experimental results on the acceleration time histories.

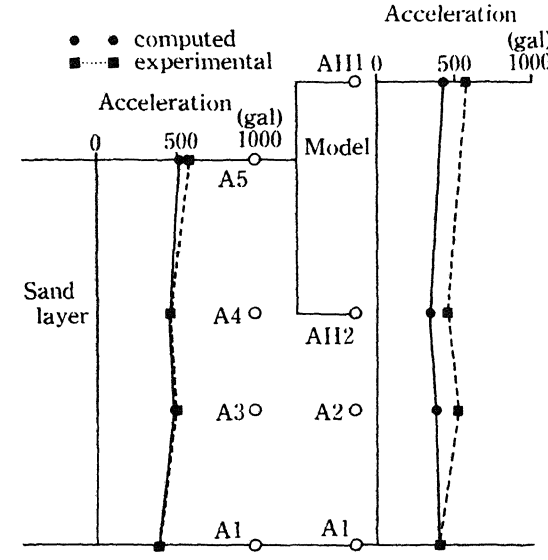

Fig.6 Comparison between computed and experimental results on the maximum acceleration.

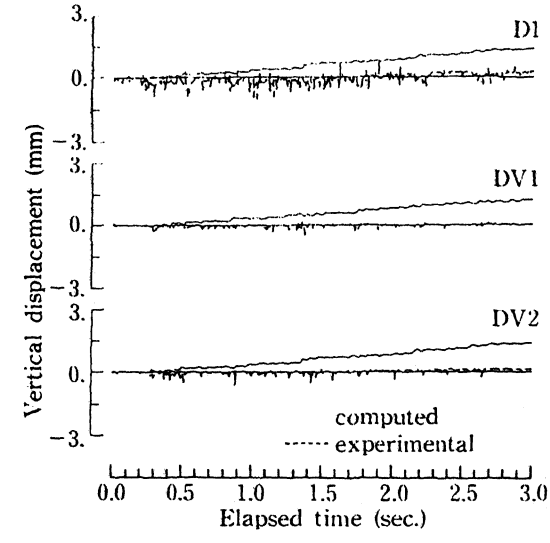

Fig.7 Comparison between computed and experimental results on the structure settlement.

experimental settlements but they are very small because of the high soil density.

Figures 8 and 9 show the pore pressure time histories. Taking the effect of the ground saturation accurately into account, the generation of pore pressure is small considering the large acceleration. The calculated pore pressures W6 and W8, which were located at the side of structure, were minus values during excitation. This is because the boundary of the buried sides of the structure were treated as fixed to the soil. However, other pore pressures under the structure were generated gradually and the tendency and values are well simulated by our analytical method.

5. CONCLUSIONS

The computed time histories for both acceleration and settlement were in good agreement with the measured results. Also, the generation of pore mater pressure was well simulated by evaluating the bulk modulus of pore water, alehough it was greatly affected by the soil saturation. This nonlinear response

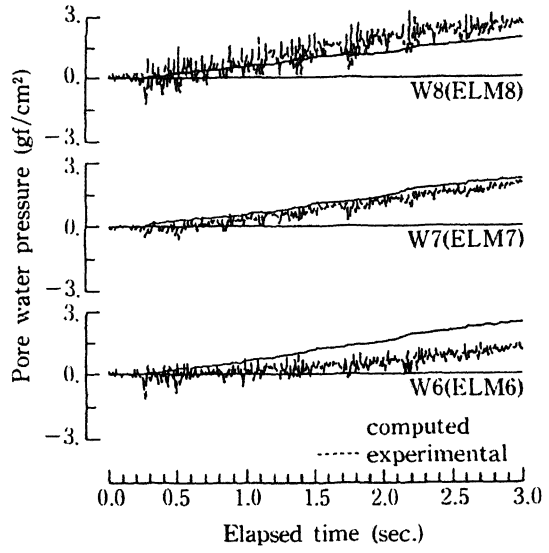

Fig.8 Comparison between computed and experimental results on the pore water pressure at underneath of the structure.

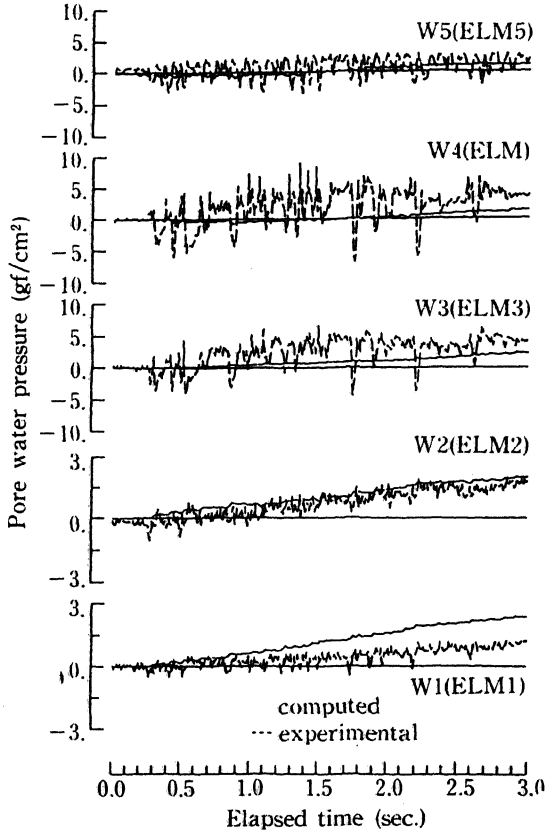

Fig.9 Comparison between computed and experimental results on the pore water pressure at side of the structure.

analytical method gives good predictions for aseismic design of the very important structures on saturated sandy ground during strong earthquakes.

REFERENCES

Ghaboussi, O. 1971. Dynamic analysis of porous elastic solids saturated with compressive fluids. EERC Report No.71-6.

Hughes, T.J.R. & Liu, W.K. 1978. Implicit-explicit finite elements in transient analysis. ASME J. of Applied Mecha. Vol.45, No.2: 375-378.

Nishi, K. & M. Kanatani 1990. Constitutive relations for sand under cyclic loading based on elasto-plasticity theory. Soils & Foundations.Vol.30, No.2: 43-59.

Sekiguchi, H. & H. Ohta 1977. Induced anisotropy and time dependency in clay. Speciality session 9, 9th ICSMFE: 229-238.

APPENDIX

The following constitutive relations were used in fhis paper.
The relation between the seress incremental tensor and total strain incremental tensor $d\varepsilon_{ij}$ is given by the following equation:

$$d\sigma_{ij} = D_{ijkl}\, d\varepsilon_{ij}$$

where,

$$D_{ijkl} = D^{E}_{ijkl} - \frac{D^{E}_{ijmn}\dfrac{\partial g}{\partial \sigma_{mn}}\dfrac{\partial f}{\partial \sigma_{pq}} D^{E}_{pqkl}}{\dfrac{\partial f}{\partial \sigma_{mn}} D^{E}_{mnpq} \dfrac{\partial g}{\partial \sigma_{pq}} - \dfrac{\partial f}{\partial \varepsilon^{p}_{mn}}\dfrac{\partial g}{\partial \sigma_{mn}}}$$

where, D^{E}_{ijkl} is an elastic matrix. Also, $\partial g/\partial \sigma_{ij}$ $\partial f/\partial \sigma_{ij}$ and h are given by the following equations, respectively:

$\eta^{*} \geq \eta^{*}_{max}$:

$$\frac{\partial g}{\partial \sigma_{ij}} = \frac{1}{M_m \sigma_m'}\left\{\frac{\eta_{ij}-\eta_{ijo}}{\eta^{*}} + (M_m-\eta^{*})\cdot\frac{\delta_{ij}}{3}\right\}$$

$$\frac{\partial f}{\partial \sigma_{ij}} = \frac{1}{\sigma_m'}\left\{\frac{\eta_{ij}-\eta_{ijo}}{\eta^{*}} - \frac{S_{ij}(\eta_{ij}-\eta_{ijo})}{\sigma_m'\eta^{*}}\cdot\frac{\delta_{ij}}{3}\right\}$$

$$h = \frac{M_m\sigma_m'}{G_o^{*}}\left(1-\frac{\eta^{*}}{M_f}\right)^{-2}$$

$\eta^{*} < \eta^{*}_{max}$:

$$\frac{\partial g}{\partial \sigma_{ij}} = \frac{1}{\sigma_m' \{\alpha (M_m - \eta_r^*) + \eta_r^*\}} \left\{ \frac{\eta_{ij} - \eta_{ijr}}{\eta^*_r} + \alpha (M_m - \eta^*_r) \frac{\delta_{ij}}{3} \right\}$$

$$\frac{\partial f}{\partial \sigma_{ij}} = \frac{1}{\sigma_m'} \left\{ \frac{\eta_{ij} - \eta_{ijr}}{\eta^*_r} - \frac{S_{ij}(\eta_{ij} - \eta_{ijr})}{\sigma_m' \eta^*_r} \frac{\delta_{ij}}{3} \right\}$$

$$h = \frac{\sigma_m' \{\alpha (M_m - \eta^*_r) + \eta^*_r\}}{G_0^*} \left(1 - \frac{\eta^*_r}{2M_f}\right)^2$$

where, η_{ij} is S_{ij}/σ_m', and α and v_{df} are given by the following equations:

$$\alpha = 1 - \frac{v_{df}}{v_{df}}$$

$$v_{df} = m^* \sigma_m' (\eta^*_r)^n$$

where S_{ij}, σ_m', v_{df} and v_{df} are the deviatoric stress tensor, the effective mean stress, the volumetric strain accumulated at the reversal point and the final volumetric strain which will be accumulated when cyclic loading is conducted under the effective stress ratio at that point. M_f, G_0^*, m^* and n are the material constant.